The Free Internet Journal for Organic Chemistry

Paper

Archive for Organic Chemistry

34 **2026**, part __, 0-0

to be inserted by editorial office

Magnetically recoverable CuI-Fe_3O_4/C catalyst - preparation and application in 1-aminoalkyl-2-naphthol synthesis

Hang Thien Thi Nguyen,[a,b] Vu Khanh Nguyen Ngo,[a,b] Thuy Hong Ngoc Phan,[a,b] Quynh Diem Le,[a,b] The Thai Nguyen,[a,b,c] Nhuan Ngoc Doan,[a,b] and Phuong Hoang Tran[a,b]*

[a]*Department of Organic Chemistry, Faculty of Chemistry, University of Science, Ho Chi Minh City, Vietnam;* [b]*Vietnam National University, Ho Chi Minh City, Vietnam;* [c]*Faculty of Interdisciplinary Science, University of Science, Ho Chi Minh City, Vietnam*

Email: thphuong@hcmus.edu.vn

Received mm-dd-yyyy **Accepted** mm-dd-yyyy **Published on line** mm-dd-yyyy

Dates to be inserted by editorial office

Abstract

The development of a novel magnetic nanocatalyst (CuI-Fe_3O_4/C), through an environmentally benign synthesis route using *Annona squamosa* peel extract, is reported. The magnetic catalyst was thoroughly characterized (FTIR, TGA, XRD, SEM-EDS, ICP-MS, and VSM), confirming the successful incorporation of copper and magnetite into the carbon matrix. The catalytic performance of CuI-Fe_3O_4/C was evaluated in a three-component synthesis of 1-aminoalkyl-2-naphthols under ultrasonic activation. Optimal conditions were achieved under solvent-free conditions, with a substrate molar ratio of 1:1:1, a reaction time of 3.5 hours, and 10 mg of catalyst, yielding up to 70% conversion. The catalyst demonstrated magnetic responsiveness, allowing for easy recovery and reuse, retaining over 56% of its catalytic activity after three cycles.

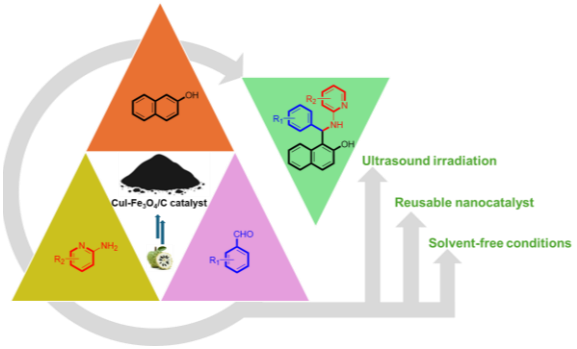

Keywords: Magnetic nanocatalyst; biomass, 1-aminoalkyl-2-naphthols; sonication; multicomponent reaction.

Introduction

Magnetite (Fe_3O_4) offers a promising approach to achieve this goal due to its magnetic properties, chemical stability, low toxicity, and cost-effectiveness.[1] Fe_3O_4-based materials are emerging as important solid supports for loading heterogeneous catalysts and immobilizing homogeneous ones. Magnetic solid catalysts are solid acid catalysts composed of Fe_3O_4 particles in their core or on their surface.[2, 3] Compared to conventional solid acids, magnetic solid acids can be more easily separated using an external magnetic field, particularly in viscous or solid reaction mixtures.[3, 4] Due to its hydrophilic nature and biocompatibility, Fe_3O_4 has attracted significant attention for a wide range of applications, including wastewater treatment, pigments, magnetic resonance imaging (MRI), and various biomedical uses. Moreover, Fe_3O_4-based magnetic materials have also found applications in environmental remediation, electrocatalysis, organic synthesis, biodiesel production, and cancer therapy.[1, 2, 5] The use of magnetic nanocatalysts is rapidly expanding as a promising approach for developing sustainable and green chemical processes. Magnetic separation eliminates the need for conventional filtration or centrifugation after the reaction, offering a practical method for catalyst recovery.

Multicomponent reactions (MCRs) serve as highly adaptable and efficient strategies within organic, medicinal, and combinatorial chemistry.[6] They are also strongly aligned with the goals of sustainable and green chemistry due to their minimized waste and resource-efficient processes.[7] These reactions are particularly valued for their atom economy and their capability to generate molecular diversity in a streamlined fashion. Unlike conventional linear synthesis routes, MCRs allow for the straightforward creation of vast chemical libraries using simple, commercially accessible reagents.[8, 9] MCRs enable the formation of target products through a one-pot process without the need to isolate intermediates, thereby reducing both energy consumption and reaction time. The most valuable MCRs also provide additional benefits, including high selectivity, synthetic convergence, and excellent atom economy, in which most or all of the reactant atoms are incorporated into the desired product. These characteristics make MCRs highly attractive and environmentally friendly synthetic tools.[8, 9]

A notable example is the Betti reaction, a multicomponent process involving aldehydes, primary aromatic amines, and phenols or naphthols, which yields α-aminobenzyl phenols via a modified Mannich-type pathway.[10, 11] The Mannich reaction is one of the most important multicomponent reactions in organic chemistry and is widely employed for the one-pot synthesis of 1-aminoalkyl-2-naphthols, commonly known as Betti bases. Initially introduced by Mario Betti in the early 1900s, this reaction remains a valuable synthetic tool.[12] The resulting products often exhibit important biological properties, such as antimicrobial, blood pressure-lowering, and heart rate-reducing effects, in addition to various pharmacological applications. These compounds serve as key precursors in the synthesis of a wide range of biologically important natural products, including antibiotics and HIV protease inhibitors.[13] Amitha and Vasudevan reported the synthesis of Betti base-functionalized zinc and copper phthalocyanines and their quaternized analogues, which exhibited strong interactions with CT-DNA and promising photophysical behavior, including efficient singlet oxygen generation and DNA cleavage activity.[14] Moreover, this class of compounds has exhibited remarkable catalytic activity, particularly as asymmetric catalysts in the enantioselective alkylation or arylation of benzaldehyde. The classical three-component Betti reaction involves the condensation of an aldehyde, ammonia or urea, and 2-naphthol. Recently, a novel approach has been reported, featuring a three-component condensation of aromatic aldehydes, 2- or 4-aminopyridine, and 2-naphthol, catalyzed by MNP-$PhSO_3H$ and [1,4-DHPyrazine][$C(NO_2)_3$]$_2$.[15, 16] The resulting 1-aminoalkyl-2-naphthols are an important class of organic compounds referred to as Betti bases. Studies on the chemical properties of Betti bases date back to the early 20th century, when Betti first described the synthesis of 1-aminobenzyl-2-naphthols. Betti base compounds,

particularly 1-aminoalkyl-2-naphthols, are highly suitable for chemical sensing applications. When a Betti base is coupled with 4-nitrophthalonitrile under base-catalyzed conditions in the presence of K_2CO_3, the reaction yields a modified phthalonitrile derivative: 4-((1-phenyl(pyridin-2-ylamino)methyl)naphthalen-2-yl)oxy)phthalonitrile (BBPN). Both the Betti base and BBPN exhibit metal ion sensing capabilities, showing selective fluorescence enhancement in the detection of Hg^{2+} and Cr^{3+} ions.[17]

In recent years, the multicomponent condensation of aldehydes with β-naphthol and amide/amine derivatives has emerged as an efficient approach for synthesizing 1-amidoalkyl-2-naphthols.[18] An efficient three-component protocol for the synthesis of aminonaphthols (Betti bases) without the use of any catalyst was described by Ghandi and co-workers, in which 2-naphthol, aromatic aldehydes, and heteroaryl amines react smoothly in water at ambient temperature.[19] Many studies on the synthesis of 1-aminoalkyl-2-naphthols using various types of homogeneous and heterogeneous catalysts have been reported, such as $SnCl_4{\cdot}5H_2O$, polymer-supported sulfonic acid, ionic liquids, nano-sulfated zirconia, $[HMIM]C(CN)_3$, $ZrO(OTf)_2$, and $Bi(NO_3)_3.5H_2O$.[20-27] Despite their usefulness, many of these catalytic systems still suffer from certain drawbacks, such as prolonged reaction times, moderate yields, harsh conditions, the need for toxic, corrosive, costly, non-recyclable or difficult-to-handle catalysts in relatively large amounts, excessive use of acetamide, and labor-intensive work-up procedures.[28, 29] For this reason, significant attention has been directed towards developing environmentally benign processes and employing recyclable catalysts with high efficiency for the synthesis of 1-amidoalkyl-2-naphthols and 1-(α-aminoalkyl)-2-naphthols. Over the past decades, numerous methodologies have been developed for this transformation, including catalyst-free conditions, solvent-free protocols, and the use of various homogeneous and heterogeneous catalytic systems such as Brønsted acids, Lewis acids, ionic liquids, and supported metal catalysts.[30] In particular, magnetically recoverable catalysts based on Fe_3O_4 have been extensively explored owing to their facile separation and reusability.[31] An immobilized molybdenum Schiff-base complex supported on Fe_3O_4 has been developed as a heterogeneous nanocatalyst, which was successfully applied to the synthesis of 1-(α-aminoalkyl)-2-naphthol and α-aminonitrile derivatives under mild and environmentally friendly conditions, as reported by Rakhtshah and co-workers.[32] Despite these advances, many reported systems still suffer from certain limitations, including the use of non-renewable catalyst precursors, harsh reaction conditions, difficulty in catalyst recovery, or limited sustainability.

One-pot catalytic strategies using readily available, non-toxic, and inexpensive reagents are particularly appealing since they shorten reaction times, avoid the isolation of intermediates, and minimize both energy and material consumption. Considerable research efforts have therefore been devoted to designing new multicomponent reactions. From the perspective of green chemistry, advancing clean synthetic technologies is essential, and the use of heterogeneous catalysts, as well as solvent-free protocols, is recognized as an effective way to reduce the environmental footprint of chemical processes.[33] Nanocatalysts, in particular, provide distinct benefits, including higher activity, enhanced stability, recyclability, straightforward recovery, and lower cost, making them attractive substitutes for conventional catalysts.[34]

Therefore, in this study, CuI-Fe_3O_4/C catalyst was prepared and applied to synthesize 1-aminoalkyl-2-naphthols *via* a three-component reaction between amine, aldehyde, and naphthol. In recent years, increasing attention has been directed toward the development of environmentally benign catalytic systems derived from renewable biomass resources. Biomass-derived carbon materials have emerged as promising catalyst supports due to their low cost, tunable surface properties, and sustainable origin. In this context, the integration of biomass-derived carbon with magnetically recoverable metal-based catalysts offers an attractive strategy for designing efficient and green catalytic systems. Such hybrid materials not only combine catalytic activity with easy recyclability but also align well with the principles of green chemistry. We herein

report the preparation of a novel CuI-Fe_3O_4/C magnetic nanocatalyst using *Annona squamosa* peel extract as a renewable carbon source. The catalyst was successfully applied to the solvent-free synthesis of 1-aminoalkyl-2-naphthols via a three-component Betti reaction under ultrasonic irradiation. Compared with previously reported systems, the present approach provides advantages in terms of catalyst sustainability, operational simplicity, and magnetic recyclability, while maintaining reasonable catalytic efficiency.

Results and Discussion

Initially, the solid supported catalyst from the Annona squamosa peel extract was prepared according to the procedure described in the experimental section. The Annona squamosa peel are available from Tay Ninh province, Vietnam.

Characterization of CuI-Fe_3O_4/C

FTIR spectral analysis was performed to identify the functional groups present in the synthesized samples, as shown in **Figure 1**. A broad absorption band observed around 3372 cm^{-1} corresponds to the O–H stretching vibrations of hydroxyl groups in the material. The peak at 1610 cm^{-1} was attributed to the stretching vibrations of conjugated carbon–carbon double bonds (C=C). Additionally, the absorption band at 1393 cm^{-1} was associated with C–H deformation vibrations typical of cellulose and hemicellulose structures. The peak observed near 970 cm^{-1} was assigned to the C–O stretching vibrations. The signal at 570 cm^{-1} of the samples was reported to be related to the vibration of metal oxide bonds.[35, 36]

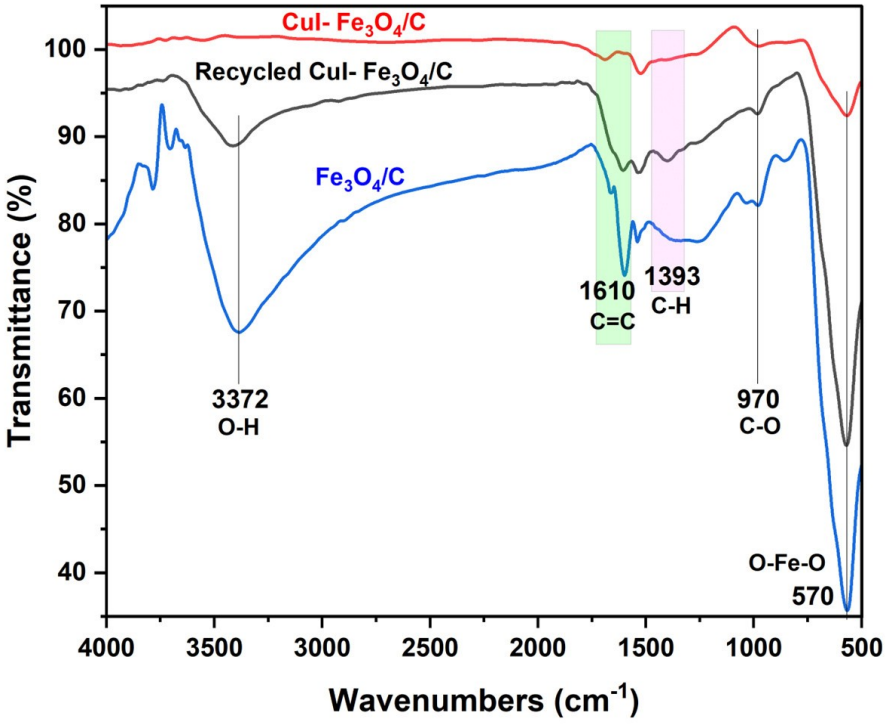

Figure 1. FTIR spectra of CuI-Fe_3O_4/C, Fe_3O_4/C and recycled catalyst

The XRD pattern was used to evaluate the crystallinity of CuI-Fe_3O_4/C. As shown in **Figure 2**, the XRD spectrum with a broad peak at 25° was that of amorphous carbon, a sample that displayed five diffraction peaks at around 30.4, 35.7, 43.7, 57.6, 63.0° corresponding to the crystal planes (220), (311), (400), (511), (440) of Fe_3O_4. There were sharp and distinct peaks a 25.7, 29.6, 42.4, 50.2, and 61.4° corresponding to the

crystal planes (111), (200), (220), (311), and (440) of CuI. The presence of these peaks was in agreement with JCPDS 19-0629 and JCPDS 06-0246, indicating high purity of the crystals Fe_3O_4 and CuI.[37, 38]

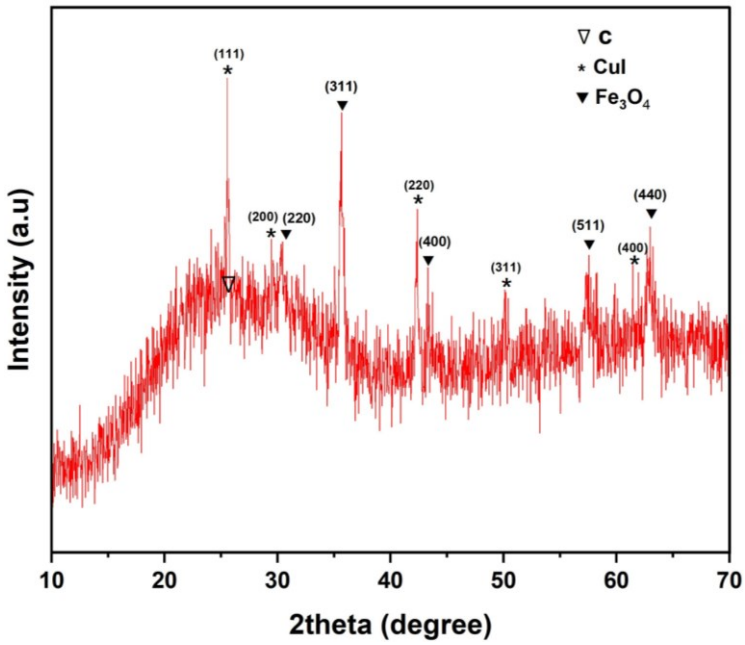

Figure 2. X-ray diffraction pattern of CuI-Fe_3O_4/C

Figure 3 illustrates the thermal behavior of the CuI–Fe_3O_4/C catalyst during pyrolysis at various temperatures, as determined by TGA analysis under an air atmosphere. The thermal decomposition process occurs in three distinct stages. Initially, the material exhibited a minor weight loss of approximately 2.5% between room temperature and 300 °C, likely due to the desorption of physically adsorbed water and other volatile components. A significant mass reduction of about 23.5% was observed between 300 and 500 °C, corresponding to the thermal degradation of organic components. The continuous weight loss in this range was attributed to the decomposition of amorphous carbon and the condensation of Fe_3O_4. At around 450°C, major biomass constituents, such as cellulose and lignin, undergo substantial decomposition. After heating to 500 °C, approximately 72% of the original mass remained, indicating the stability of the Fe and Fe_3O_4 content under a nitrogen atmosphere. Additionally, the presence of CuI in the biomass may have contributed to the thermal stability, as it did not decompose significantly at this temperature.

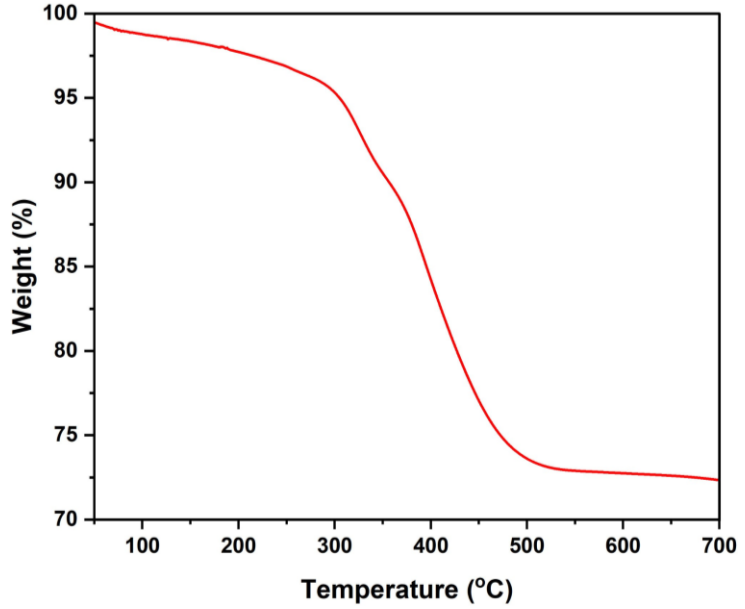

Figure 3. TGA diagram of CuI-Fe_3O_4/C

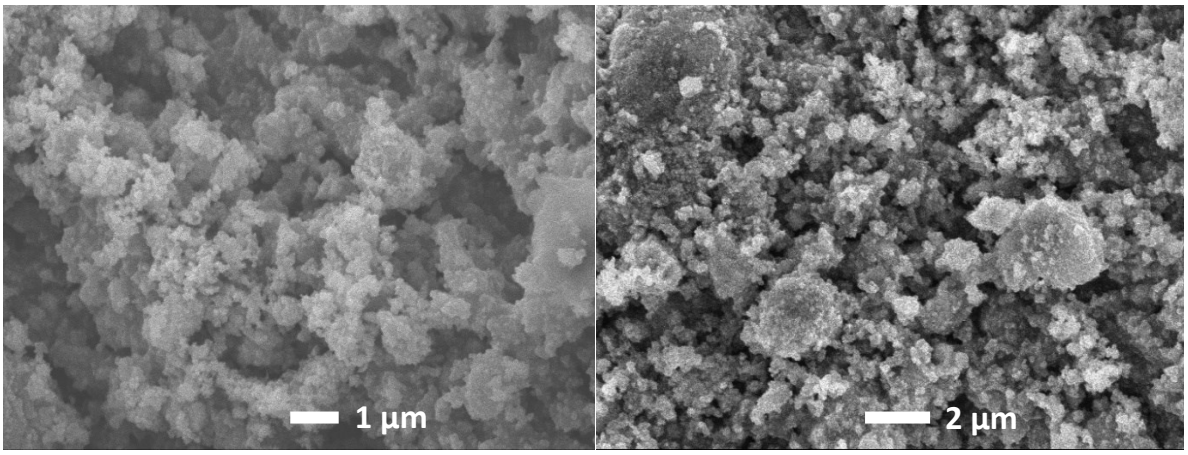

a)

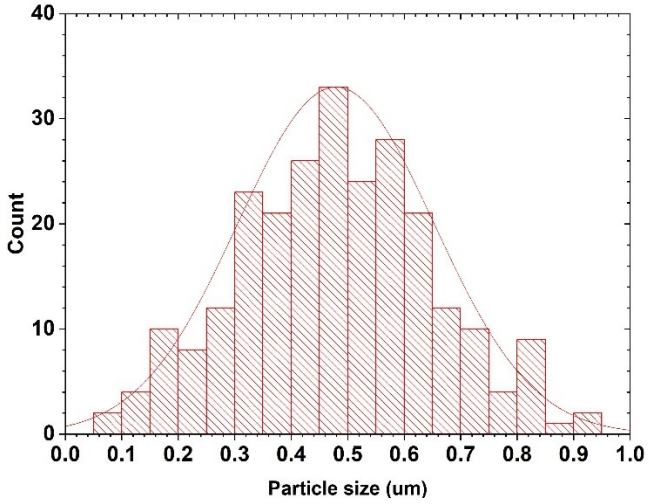

b)

Figure 4. a) SEM images and b) Particle size distribution of CuI-Fe_3O_4/C

Scanning Electron Microscopy (SEM) provides high-magnification and high-resolution imaging by scanning the sample surface, allowing for detailed observation of the material's morphology. As depicted in **Figure 4a**, the CuI–Fe_3O_4/C composite displays considerable agglomeration, with rough surface textures and a broad distribution of particle sizes. Based on the SEM image in **Figure 4b**, the average particle size was estimated to range from approximately 0.3 to 0.6 µm.

Energy-Dispersive X-ray Spectroscopy (EDS) is a material composition analysis technique that identifies elemental constituents by detecting the characteristic X-ray spectrum emitted from a sample when it interacts with an electron beam. This technique provides both qualitative and quantitative information about the elements present in the CuI–Fe_3O_4/C catalyst. The EDS spectrum (**Figure 5**) revealed that the material is primarily composed of carbon and oxygen, with a strong oxygen signal followed by a carbon signal, indicating the purity of the composite. The presence of Fe confirmed successful incorporation of Fe_3O_4, while the detection of trace amounts of Cu and I demonstrated the successful attachment of CuI to the Fe_3O_4/C support. These results confirm the successful synthesis of the CuI–Fe_3O_4/C catalyst.

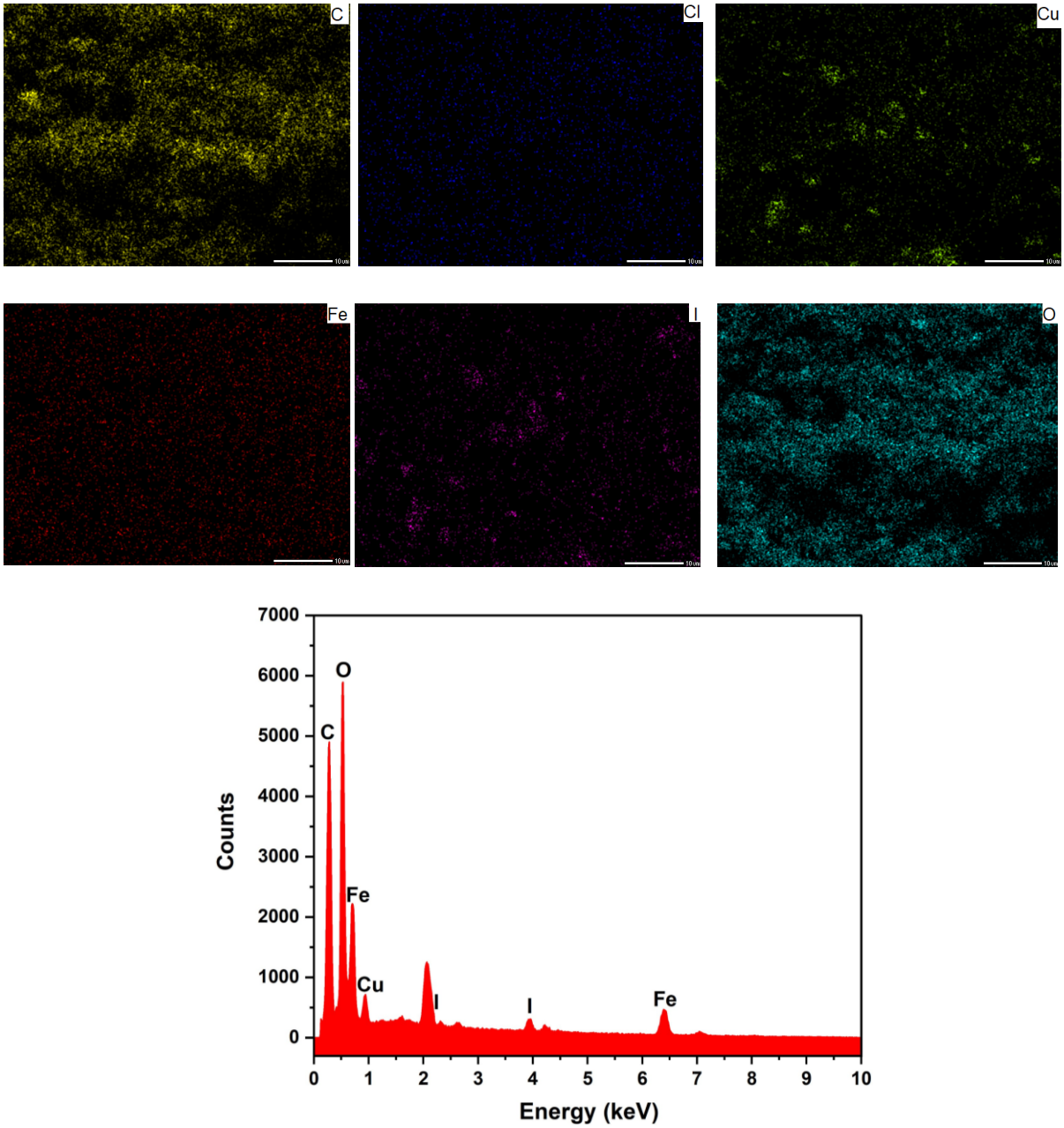

Figure 5. Mapping images and EDS spectra of CuI-Fe_3O_4/C

The more accurate Fe content was determined to be 6.129 mmol.g^{-1} and the Cu content to be 0.558 mmol.g^{-1}, according to ICP-MS analysis. Hysteresis is an irreversible phenomenon between the magnetization and reversal process in ferromagnetic materials due to the ability of ferromagnetic materials to retain magnetism. The phenomenon of hysteresis is an important and most visible characteristic of ferromagnetic substances. When placing this material in a strong magnetic field, a strong magnetic field will appear in the material. After removing the external magnetic field, the material still retains this strong magnetic field and acts as a permanent magnet. The use of external magnetic methods can influence the magnetic field of materials.

The magnetization curves of the three samples at room temperature were shown in **Figure 6**. In the Fe_3O_4/C sample, the carbonation of Fe-impregnated biomass produced significant magnetism. After the process of attaching CuI to the Fe_3O_4/C sample, we obtained the CuI-Fe_3O_4/C sample, as indicated by the results, which showed that the sample remained magnetic. The recovered sample exhibited the highest magnetic response, which may be attributed to the presence of magnetic Fe_3O_4 and the carbonization process

occurring during treatment. This suggests that magnetic properties were enhanced in the washed and processed catalyst. From the above results, it can be demonstrated that the catalyst was magnetic, allowing for easy separation of the catalyst from the reaction by applying an additional magnetic field. However, during catalytic reactions and recycling, organic residues, solvents, or amorphous carbon coating on Fe_3O_4 particles may be partially removed. This exposes more of the Fe_3O_4 core, effectively increasing the magnetic mass fraction.

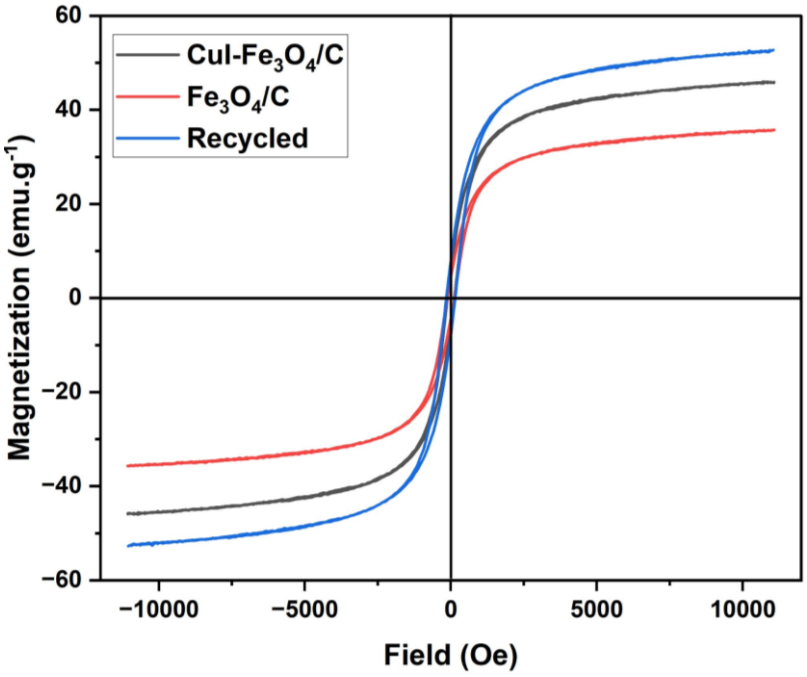

Figure 6. Magnetization curves of three samples at room temperature

Investigation of MCR reaction conditions

In this study, the synthesis of 1-aminoalkyl-2-naphthol was chosen to evaluate the efficiency of the catalyst. To determine the optimal reaction conditions, a model reaction involving 4-fluorobenzaldehyde, 2-aminopyridine, and 2-naphthol was employed (**Figure 7**).

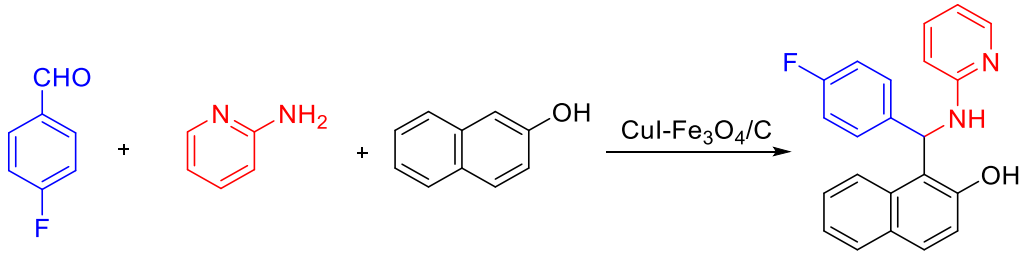

Figure 7. Synthesis reaction of -((4-fluorophenyl)(pyridine-2-ylamino)methyl) naphthalene-2-ol

To investigate the influence of the solvent on the product yield, the initial condition tested was a substrate ratio of 4-fluorobenzaldehyde:2-naphthol:2-aminopyridine = 1:1:1 (mmol), under ultrasound irradiation for 90 minutes using the CuI-Fe_3O_4/C catalyst. The results are presented in **Figure 8.** When the reaction was carried out in nonpolar protic solvents, such as acetone and ethyl acetate, the product yield was relatively low. The reaction also produced relatively low yields in nonpolar solvents such as xylene and toluene. In contrast, solvents with moderate to high polarity, such as ethanol (EtOH), methanol (MeOH), and water (H_2O), resulted in higher reaction efficiency compared to non-protic polar solvents.

According to the experimental results, the reaction exhibited the highest efficiency under solvent-free conditions. This observation is consistent with previous reports, which have also shown that solventless conditions often lead to high product yields. During the reaction, the product solidified immediately, and in the presence of a solvent, the solid product exhibited limited solubility. This reduced solubility likely contributed to the lower efficiency observed in solvent-based reactions. In contrast, the solvent-free condition provided the best performance and was therefore selected for further investigation.

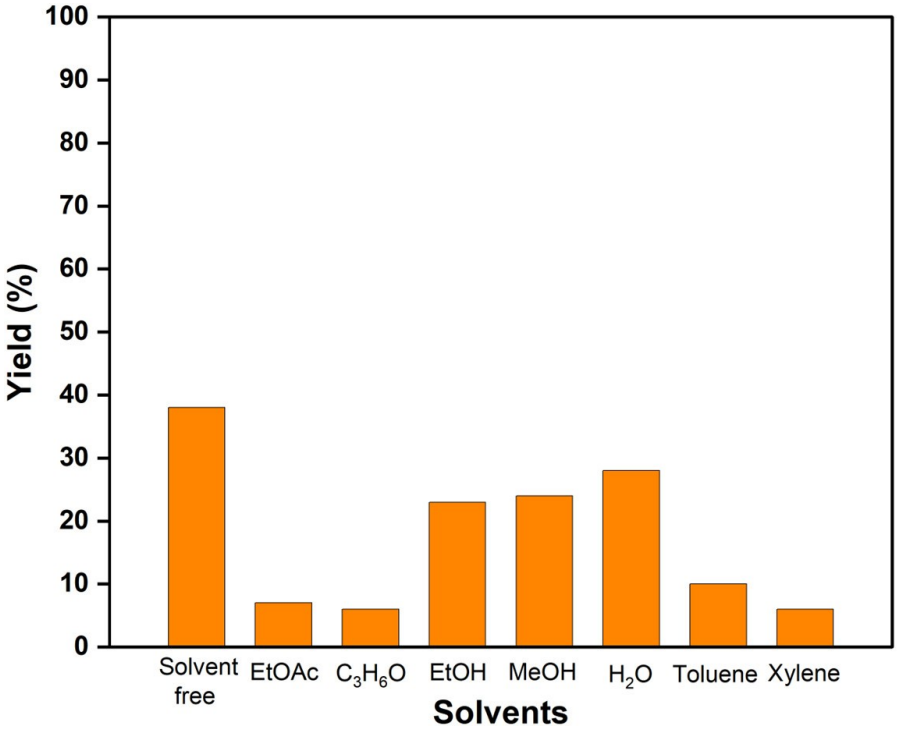

Figure 8. The effect of the solvent on reaction yield

As shown in **Figure 9**, the reaction achieved a yield of 23% within the first 30 minutes. The efficiency increased gradually over time, with only a modest improvement of approximately 5–7% between 1 and 3 hours. This limited increase is likely due to insufficient reaction time for complete product formation under the given conditions. Extending the reaction time to 3.5 hours resulted in a significant increase in yield, reaching 70%, indicating that this was the optimal duration for product synthesis. However, further increasing the reaction time to 4 hours led to a noticeable decline in efficiency, with the yield dropping to 49%. The reaction efficiency continued to decline when the reaction time was extended to 4.5 hours. This decrease may be attributed to the occurrence of side reactions over prolonged durations, which likely reduced the yield of the desired product. Based on these observations, 3.5 hours was selected as the optimal reaction time.

To investigate the influence of the catalyst on the reaction, the following conditions were applied: ultrasonic irradiation for 3.5 hours under solvent-free conditions, with a catalyst mass of 10 mg, and a molar ratio of 4-hydroxybenzaldehyde:2-naphthol:2-aminopyridine of 1:1:1. According to **Figure 10**, all iron-containing catalysts exhibited relatively high efficiencies. Among them, CuI-Fe_3O_4/C achieved the highest yield at 70%, while Fe_3O_4/C provided a yield exceeding 60%. These results highlight the significant role of iron in enhancing the reaction efficiency. Compared to two other types of catalysts from peel extract, (ZnO/C) and (NiO/C), the product yield was also relatively high, particularly in the presence of iron. In comparison, the yield obtained using copper(I) iodide alone was relatively low. This may be attributed to the large particle size of copper(I) iodide, which could hinder effective interaction with the reactants and limit product formation.

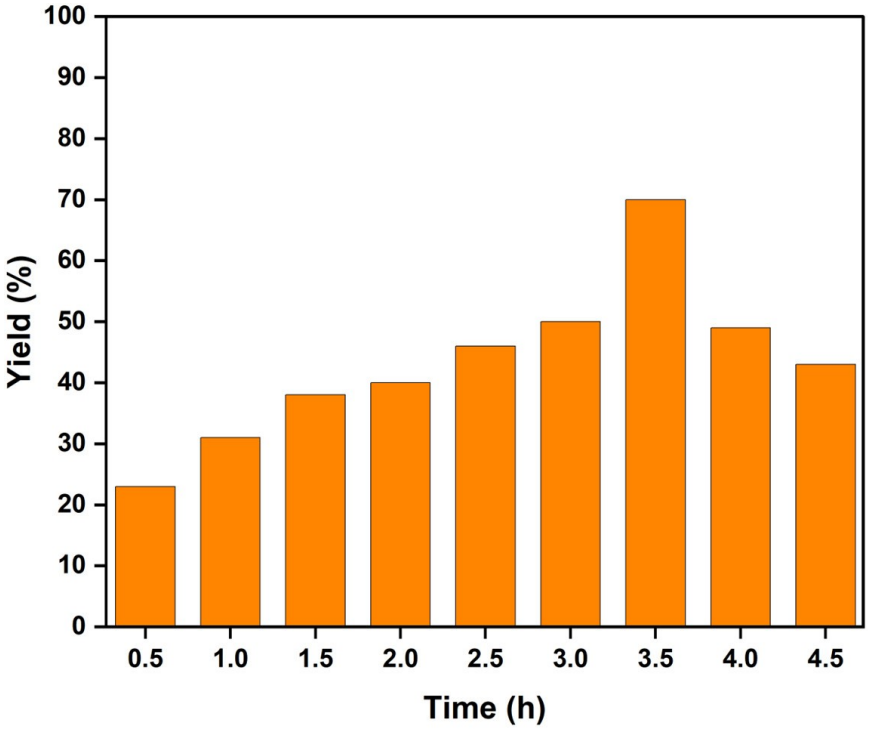

Figure 9. The effect of reaction time on product yield

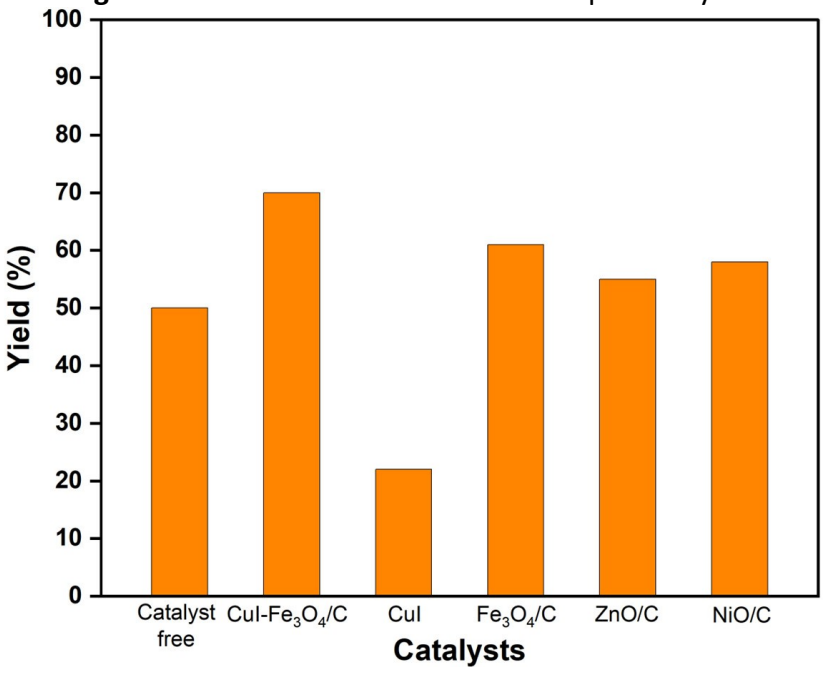

Figure 10. The effect of the catalyst on product yield

Through the optimization of reaction conditions, the target product 4a was obtained in high yield. The synthesis of 1-aminoalkyl-2-naphthol derivatives was successfully carried out under the following optimized conditions: a molar ratio of 4-fluorobenzaldehyde:2-naphthol:2-aminopyridine = 1:1:1 (mmol), solvent-free environment, ultrasonic irradiation for 3.5 hours, and 10 mg of CuI-Fe_3O_4/C catalyst.

Synthesis of 1-aminoalkyl-2-naphthol derivatives

Based on the optimization of reaction conditions, the desired products were successfully synthesized, and the reaction efficiency for producing 1-aminoalkyl-2-naphthol derivatives was evaluated (**Table 1**). The synthesized products exhibited varying yields depending on the nature of the substituents on the aromatic aldehydes (R^1)

and amines (R^2). Among the compounds, 4a (R^1 = 4-F, R^2 = 2-aminopyridine) and 4d (R^1 = H, R^2 = 2-aminopyridine) afforded relatively high yields of 70% and 68%, respectively. The introduction of electron-withdrawing groups, such as -Cl (4g) and -Br (4b), resulted in moderate yields of 43% and 47%, respectively. Conversely, compounds 4c (2-CH_3) and 4k–4l bearing electron-donating substituents such as –CH_3 and –OCH_3 on the benzene ring showed notably lower yields, ranging from 3% to 29%. This suggests that both steric hindrance and electronic effects significantly influence the reaction efficiency. Notably, benzamide derivatives (4j–4l) exhibited poor conversions, possibly due to the reduced nucleophilicity of the amino group in benzamide. In general, 2-aminopyridine derivatives showed better performance than benzoic acid analogs in this synthetic transformation under solvent-free conditions.

Table 1. Synthesis of 1-aminoalkyl-2-naphthol derivatives.[a]

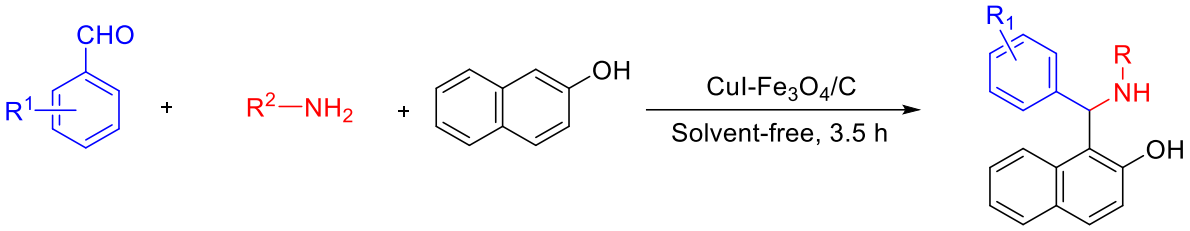

1 2 3 4

Product	R^1	R^2	Melting point (°C)		Yield (%)
			Ref	This work	
4a	4-F	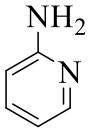	-	185 – 187	70
4b	4-Br	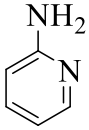	194-196[39]	194 – 196	47
4c	2-CH_3	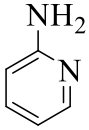	-	150 –152	23
4d	-H	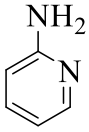	170 – 172 [22]	175 – 177	68
4e	4-CH_3	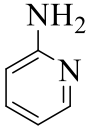	172 – 174 [22]	170 - 172	40
4f	-OCH_3	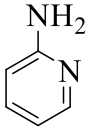	168 – 170[15]	164 – 168	8
4g	-Cl	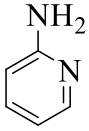	188 – 190 [15]	185 – 188	43

4h	-H	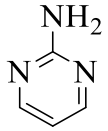	231 – 233[40]	233 – 235	63
4i	-H	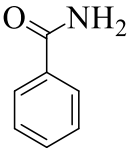	160 – 162[40]	248 – 249	23
4j	4-CH_3	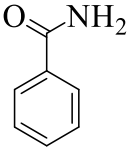	206 – 208[40]	224 – 225	trace
4k	4-OCH_3	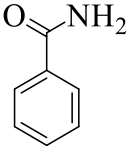	204 – 206[41]	216 – 217	trace
4l	4-F	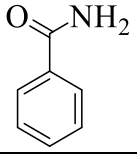	192–194[29]	229 – 230	29

[a] Reaction conditions aldehyde:2-naphthol:2-aminopyridine = 1:1:1 (mmol), 10 mg CuI-Fe_3O_4/C, solvent-free, ultrasound irradiation for 3.5 h

Proposed mechanism

In the first step of the reaction, the aldehyde contains a carbonyl (C=O) group, where the oxygen atom possesses two lone pairs of electrons. These electrons readily coordinate with the CuI-Fe_3O_4/C catalyst, which, due to the presence of iron oxide, acts as a Lewis acid capable of accepting electron pairs. Meanwhile, 2-aminopyridine contains an $–NH_2$ group with a lone pair of electrons that can nucleophilically attack the electrophilic carbon of the aldehyde's C=O group. This nucleophilic addition leads to a condensation reaction between the aldehyde and 2-aminopyridine, resulting in the formation of an imine intermediate. Rapid formation of the imine intermediate between the aldehyde and amine under Lewis acidic activation by the catalyst. The proposed reaction mechanism was illustrated in **Figure 11.**

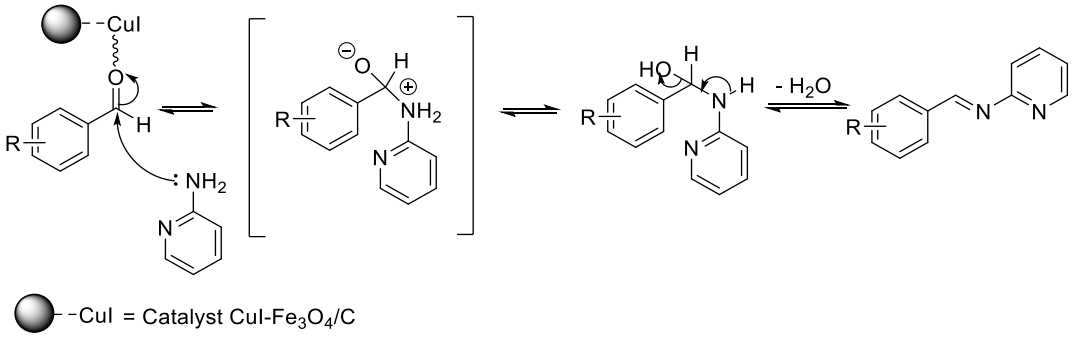

Figure 11. Stage 1 of the reaction mechanism produces 1-aminoalkyl-2-naphthols

In the next step, the hydroxyl group of 2-naphthol becomes activated, and its adjacent π-system facilitates a nucleophilic attack on the electrophilic carbon of the imine (C=N) formed in the first step. The electron density on the C=N bond is polarized toward the nitrogen atom, enhancing the electrophilicity of the

carbon. This interaction promotes the nucleophilic addition of 2-naphthol to the imine. Activation of the imine carbon (C=N) by the CuI-Fe_3O_4/C catalyst, which enhances its electrophilicity. The high nucleophilicity of 2-naphthol, particularly at the ortho-position relative to the hydroxyl group, facilitates its addition to the activated imine. Simultaneously, a proton transfer occurs via water molecules, facilitating the stabilization of intermediates. The resulting intermediate undergoes protonation and tautomerization, ultimately leading to the formation of the final 1-aminoalkyl-2-naphthol product. The process is presented in **Figure 12.** Under solvent-free conditions, limited molecular mobility and product precipitation may shift the equilibrium toward the desired product.

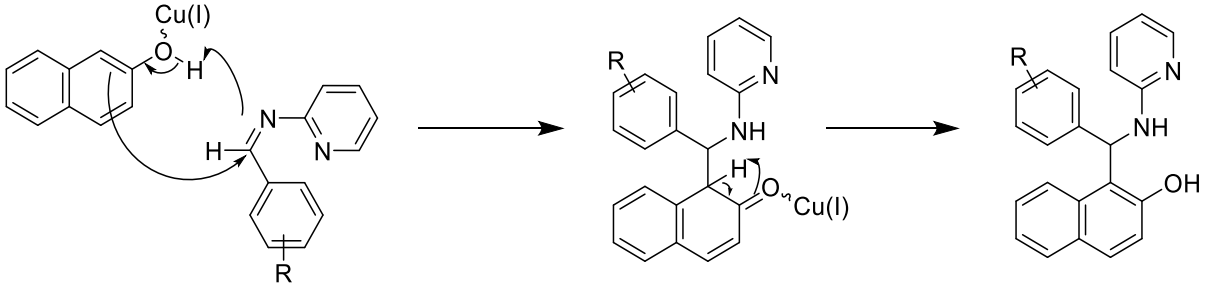

Figure 12. Stage 2 of the reaction mechanism produces 1-aminoalkyl-2-naphthols

To gain deeper insight into the reaction mechanism, we first examined the reaction between an aldehyde and 2-naphthol. However, no noticeable progress was observed even after several hours. In contrast, when the preformed Schiff base, resulting from the condensation of an amine with an aldehyde, was reacted with 2-naphthol under similar conditions, the corresponding Betti base (1-aminoalkyl-2-naphthol) was successfully obtained. These observations suggest that, in the one-pot multicomponent reaction, the imine intermediate generated in situ from the amine and aldehyde subsequently undergoes nucleophilic addition with 2-naphthol to afford the 1-aminoalkyl-2-naphthol derivatives.

Recycling of the catalyst

The reusability of the catalyst for the reaction to create 1-aminoalkyl-2-naphthols was also investigated. According to the presented data, after four reactions (three cycles), the reaction efficiency decreased significantly. This demonstrated the potential of catalysis for reuse and its contribution to green chemical processes.

Table 2. Effect of reused catalyst on reaction performance

Cycle	Product mass (g)	Yield (%)
0	0.3056	70%
1	0.2317	62%
2	0.2110	60%
3	0.1996	56%

To further evaluate the reusability and structural stability of the catalyst, ICP-MS analysis was performed on the recovered CuI-Fe_3O_4/C material after three consecutive reaction cycles. The Cu content was determined to be 0.425 mmol·g^{-1}, compared to 0.558 mmol·g^{-1} for the fresh catalyst. This corresponds to only a moderate decrease in Cu loading, indicating that most of the active Cu species are retained within the catalyst matrix during repeated use. The limited loss of metal content suggests minimal leaching under the reaction conditions and correlates well with the relatively stable catalytic performance over multiple cycles, confirming the robustness and recyclability of the catalyst system.

Conclusions

A magnetically recoverable CuI-Fe_3O_4/C nanocatalyst was successfully synthesized using a green route from *Annona squamosa* peel extract and applied in the solvent-free synthesis of 1-aminoalkyl-2-naphthols. The reaction conditions were optimized to maximize yield, and the highest product yield (70%) was obtained after 3.5 h of sonication with 10 mg of catalyst under solventless conditions. Its magnetic properties facilitated straightforward separation and reuse without significant loss in catalytic activity. The catalyst demonstrated good reusability, maintaining a reasonable efficiency after three cycles, which highlights its potential for sustainable synthesis. This work demonstrates the effective integration of green chemistry principles with multicomponent reaction strategies, offering a practical pathway for the synthesis of complex heterocycles using renewable biomass-derived materials.

Experimental Section

General

Chemicals. 2-Aminopyridine (purity ≥ 99%) and 2-aminopyrimidine (purity ≥ 99%) were purchased from Sigma-Aldrich. 4-Bromobenxaldehyde (purity ≥ 99%), 4-fluorobenzaldehyde (purity ≥ 99%), 4-hydroxylbenzaldehyde (purity ≥ 99%), 4-methoxylbenzaldehyde (purity ≥ 99%), acetone (purity ≥ 96%), benzaldehyde (purity ≥ 99%), indole (purity ≥ 99%), iron(III) chloride (purity ≥ 97%), methanol (purity ≥ 99%), *o*-tolualdehyde (purity ≥ 99%), phenyl acetylene (purity ≥ 97%), sodium hydroxyl (purity ≥ 99%), *t*-butyl isocyanide (purity ≥ 99%), 2-naphthol (purity ≥ 99%), were purchased from Macklin. Toluene (purity ≥ 99%), xylene (purity ≥ 99%), hexane (purity ≥ 96%), ethanol (purity ≥ 99%), and ethyl acetate (purity ≥ 96%) were obtained from Xilong.

Equipment. Fourier Transform Infrared (FTIR) spectroscopy was performed using a Jasco FT-IR 6600 Type A spectrometer, operating in the range of 400–4000 cm^{-1}. Thermogravimetric analysis (TGA) of the dried sample was conducted on an STA PT 1600 instrument under an inert gas atmosphere, with a heating rate of 10 °C min^{-1} from 35 to 800 °C. The crystallinity of the synthesized powders was analyzed using a Bruker D8 Advance powder X-ray diffractometer (P-XRD) with CuKα radiation (λ = 0.15418 nm), employing a step size of 0.01° and a dwell time of 0.25 s per step. Scanning electron microscopy (SEM) coupled with energy-dispersive X-ray spectroscopy (EDS) mapping was performed using a JMS-IT200 (JEOL, Japan). Inductively coupled plasma mass spectrometry (ICP-MS) analysis was carried out with an Agilent 7700x instrument. Magnetization measurements were conducted using a vibrating sample magnetometer (VSM) over a magnetic field range of –11,000 to +11,000 Oe at room temperature.

Preparation of Fe_3O_4/C

The schematic for preparing *Annona squamosa* aqueous extract and the biogenic synthesis procedure of Fe_3O_4/C are presented in **Figure 13.** The *Annona squamosa* peel was washed four times with tap and distilled water to remove dirt and flesh, then drained, dried, and ground into powder. Then, 5 g of dried peel was added to a 200 mL flask containing 100 mL of a 1:1 ethanol-distilled water mixture. This mixture was heated at 90 ℃ for 4 h. After boiling, the mixture was filtered through filter paper to obtain the extract from *Annona squamosa* peel. An aqueous extract of *Annona squamosa* peel was heated to 80 °C and stirred continuously for 1 hour. Subsequently, a 3% $FeCl_3$ solution was added to the heated extract. Upon addition, the solution color changed from greenish to black, indicating the interaction of Fe^{3+} ions with organic compounds in the extract. This led to the formation of Fe(III) complexes, which were subsequently reduced to Fe(II) and

zerovalent Fe, typically responsible for the observed color change. The reaction mixture was treated with 0.1 N NaOH, dried at 100 °C for 10 hours, and then calcined at 700 °C for 1 hour. The resulting black solid weighed 2.5 g, corresponding to a yield of 31%.

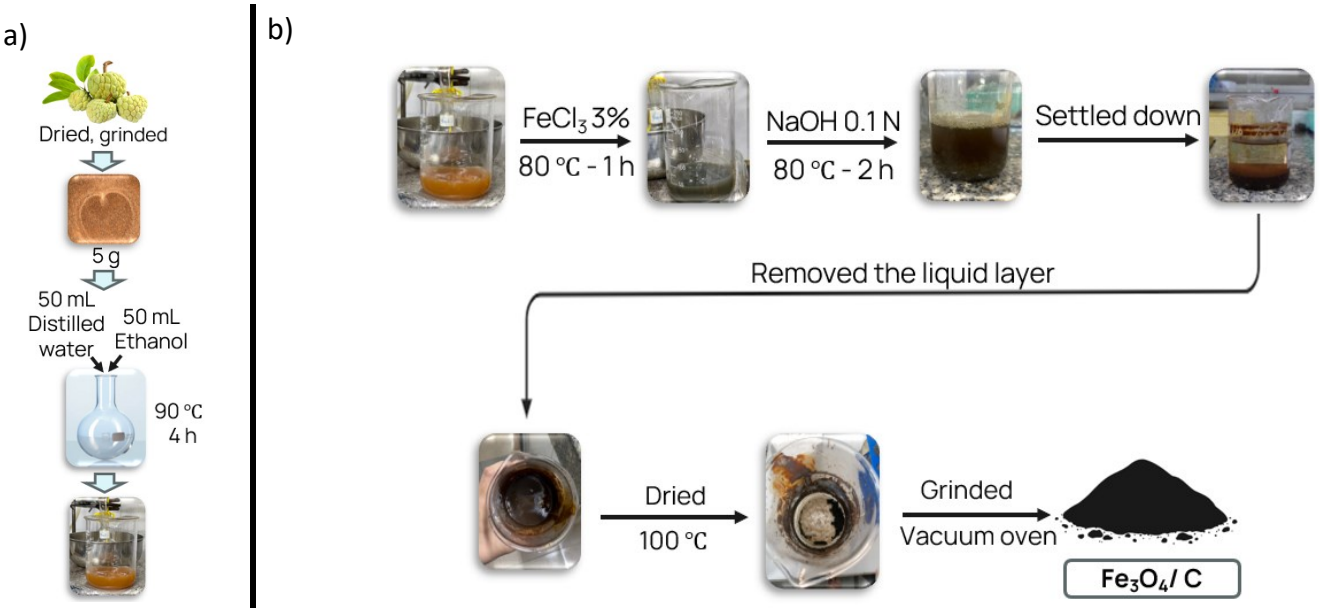

Figure 13. Schematic representation for (a) Preparation of *Annona squamosa* peel aqueous extract, (b) Preparation of Fe_3O_4/C

Preparation of CuI-Fe_3O_4/C

Subsequently, a suspension of 0.190 g CuI in 5 mL methanol (beaker A) was prepared. Separately, 1 g of Fe_3O_4/C was dispersed in 50 mL of methanol (beaker B) and sonicated. After 30 minutes, the contents of beaker A were added to beaker B (**Figure 14**). The resulting mixture (A + B) was further sonicated for 12 hours to yield the CuI–Fe_3O_4/C catalyst. The resulting CuI–Fe_3O_4/C composite was separated using an external magnet and sequentially washed with distilled water, ethanol, and acetone. It was then dried at 60 °C for 6 hours. The catalyst was characterized using TGA, XRD, SEM, EDS, elemental mapping, FT-IR, VSM, and ICP-MS techniques. The obtained black solid weighed 0.7 g, corresponding to a yield of 59%.

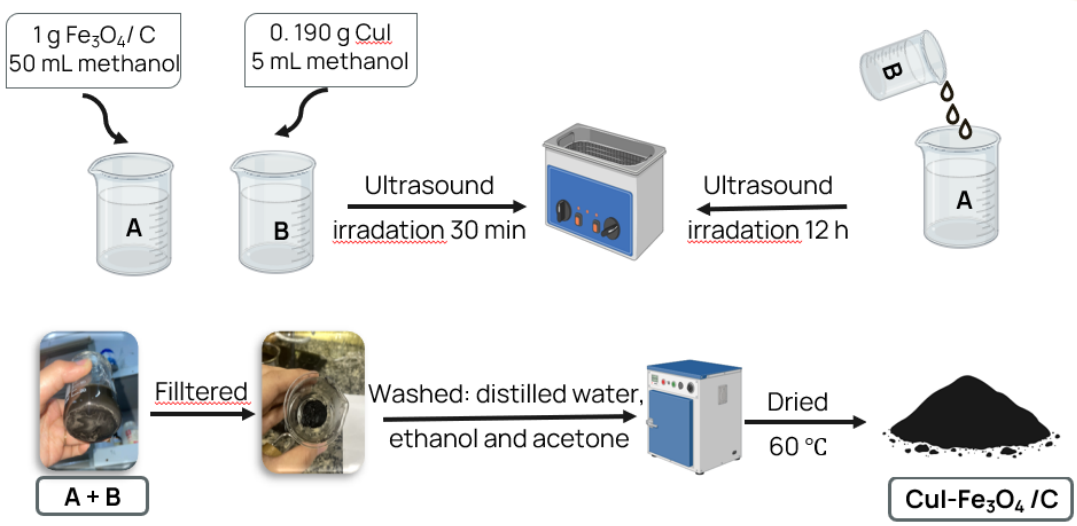

Figure 14. Schematic representation for the synthesis of CuI-Fe_3O_4/C

Synthesis of some 1-aminoalkyl-2-naphthol derivatives

A mixture of aldehyde (1 mmol), 2-naphthol (1 mmol, 0.1441 g), 2-aminopyridine (1 mmol, 0.0941 g), and CuI–Fe_3O_4/C catalyst (10 mg) was added to a 10 mL glass tube. The reaction mixture was sonicated for 3.5 h. After the reaction is complete (as confirmed by TLC), add 15 mL of ethanol to the mixture, stir at 60 °C for 10 minutes, and then remove the solid catalyst with a magnet from the solvent. The catalyst was recovered by magnetic separation, washed three times with hot ethyl acetate, and dried at 60 °C for reuse. The reaction solvent was evaporated, and the crude solid product was purified by recrystallization from hot ethanol. The mixture was cooled, filtered, and washed with cold ethanol to obtain the pure product, which was then dried and weighed to determine the yield.

1-((4-Fluorophenyl)(pyridin-2-ylamino)methyl)naphthalen-2-ol (4a)

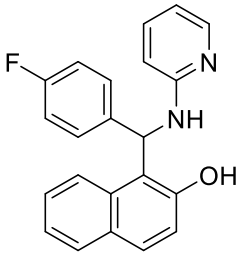

^{1}H NMR (500 MHz, DMSO) δ 10.23 (s, 1H), 7.97 – 7.76 (m, 4H), 7.38 – 7.05 (m, 10H), 6.81 (s, 1H), 6.52 (s, 1H). ^{13}C NMR (125 MHz, DMSO) δ 161.0 (d, *J* = 239.8 Hz), 158.8, 153.5, 147.7, 140.3 (d, *J* = 2.8 Hz), 137.3, 132.7, 129.6, 129.1, 129.0, 128.5 (d, *J* = 7.9 Hz), 126.7, 122.9, 120.4, 119.1, 115.0 (d, *J* = 21.2 Hz), 112.7, 109.4, 49.6. HR-MS: *m/z* $[M - H]^-$ calculated for $C_{22}H_{16}FN_2O^-$ 343.1247; found 343.1234.

1-((4-Bromophenyl)(pyridin-2-ylamino)methyl)naphthalen-2-ol (4b)[39]

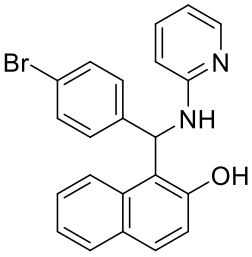

^{1}H NMR (500 MHz, DMSO) δ 10.24 (s, 1H), 7.98 – 7.79 (m, 4H), 7.40 – 7.21 (m, 4H), 7.21 – 7.16 (m, 6H), 6.84 (s, 1H), 6.54 (s, 1H). ^{13}C NMR (125 MHz, DMSO) δ 158.8, 153.5, 147.7, 144.0, 137.3, 132.7, 131.2, 129.8, 129.0, 128.9, 126.8, 122.9, 120.2, 119.2, 119.1, 112.8, 109.5, 49.7.

1-((Pyridin-2-ylamino)(o-tolyl)methyl)naphthalen-2-ol (4c)

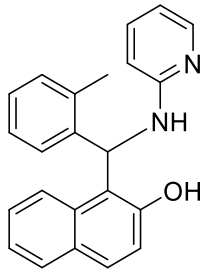

^{1}H NMR (500 MHz, DMSO) δ 10.12 (s, 1H), 8.02 (d, *J* = 6.5 Hz, 1H), 7.91 (s, 1H), 7.73 – 7.72 (m, 2H), 7.36 – 7.30 (m, 3H), 7.26 – 7.04 (m, 7H), 6.73 (s, 1H), 6.46 (s, 1H), 2.11 (s, 3H). ^{13}C NMR (125 MHz, DMSO) δ 158.5, 153.9, 147.7, 141.4, 137.1, 136.5, 133.2, 130.8, 129.4, 129.0, 128.9, 127.8, 126.8, 126.4, 125.7, 124.1 122.7, 119.1, 112.4, 109.4, 49.8, 19.6. HR-MS: *m/z* $[M + H]^+$ calculated for $C_{23}H_{21}N_2O^+$ 341.1654; found 341.1665.

1-(Phenyl(pyridin-2-ylamino)methyl)naphthalene-2-ol (4d)[22]

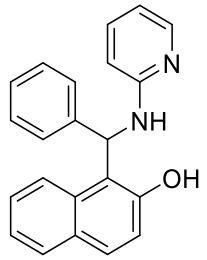

^{1}H NMR (500 MHz, DMSO) δ 10.23 (s, 1H), 7.99 – 7.96 (m, 2H), 7.79 – 7.74 (m, 2H), 7.40 – 7.33 (m, 2H), 7.26 – 7.20 (m, 8H), 7.14 – 7.11 (m, 1H), 6.82 – 6.79 (m, 1H), 6.51 – 6.49 (m, 1H). ^{13}C NMR (125 MHz, DMSO) δ 158.9, 153.9, 147.7, 144.1, 137.4, 132.8, 129.5, 129.2, 129.0, 128.4, 126.7, 126.6, 126.3, 124.2, 122.8, 120.7, 119.2, 112.6, 109.4, 50.2.

1-((4-Methylphenyl)(pyridin-2-ylamino)methyl)naphthalene-2-ol (4e)[22]

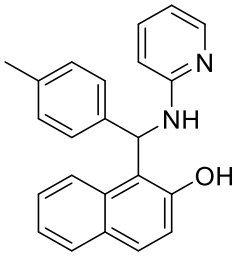

^{1}H NMR (500 MHz, DMSO) δ 10.25 (s, 1H), 7.97 – 7.95 (m, 2H), 7.78 – 7.72 (m, 2H), 7.40 – 7.36 (m, 1H), 7.25 – 7.17 (m, 5H), 7.13 (d, *J* = 8.0 Hz, 2H), 7.02 (d, *J* = 8.0 Hz, 2H), 6.79 (d, *J* = 8.5 Hz, 1H), 6.51 – 6.48 (m, 1H), 2.21 (s, 3H). ^{13}C NMR (125 MHz, DMSO) δ 158.9, 153.6, 147.7, 141.0, 137.3, 135.2, 132.8, 129.4, 129.2, 129.0, 126.6, 126.5, 124.4, 122.8, 120.8, 112.6, 109.3, 50.0, 21.0.

1-((4-Methoxyphenyl)(pyridin-2-ylamino)methyl)naphthalene-2-ol (4f)[15]

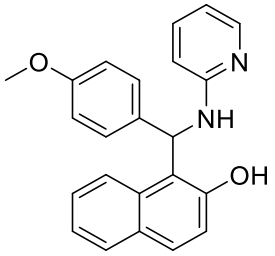

^{1}H NMR (500 MHz, DMSO) δ 10.26 (s, 1H), 7.99 – 7.95 (m, 2H), 7.78 – 7.72 (m, 2H), 7.39 – 7.34 (m, 2H), 7.25 – 7.15 (m, 6H), 6.80 – 6.77 (m, 3H), 6.49 (d, *J* = 2.0 Hz, 1H), 3.67 (s, 3H). ^{13}C NMR (125 MHz, DMSO) δ 158.9, 158.0, 153.5, 147.7, 137.4, 135.8, 132.8, 129.4, 129.2, 129.0, 127.8, 126.5, 122.8, 120.8, 119.3, 113.8, 112.6, 109.3, 55.4, 49.8.

1-((4-Chlorophenyl)(pyridin-2-ylamino)methyl)naphthalene-2-ol (4g)[15]

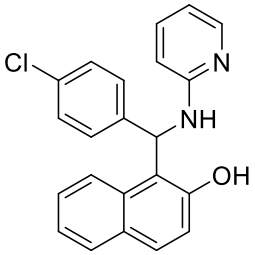

^{1}H NMR (500 MHz, DMSO) δ 10.23 (s, 1H), 7.96 – 7.81 (m, 2H), 7.80 – 7.72 (m, 2H), 7.41 – 7.38 (m, 2H), 7.29 – 7.22 (m, 8H), 6.82 (s, 1H), 6.52 (s, 1H). ^{13}C NMR (125 MHz, DMSO) δ 158.8, 153.6, 147.7, 143.5, 137.3, 132.7, 130.8, 129.7, 129.1, 129.0, 128.5, 128.3, 126.8, 124.1, 122.9, 120.2, 119.1, 112.8, 109.5, 49.7.

1-(Phenyl(pyrimidin-2-ylamino)methyl)naphthalene-2-ol (4h)[40]

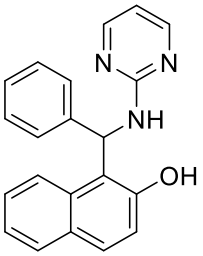

^{1}H NMR (500 MHz, DMSO) δ 10.25 (s, 1H), 8.33 (d, *J* = 4.8 Hz, 2H), 8.11 (s, 1H), 7.83 (d, *J* = 8.8 Hz, 1H), 7.78 (d, *J* = 8.8 Hz, 1H), 7.50 – 7.45 (m, 2H), 7.37 – 7.20 (m, 8H), 6.64 (t, *J* = 4.8 Hz, 1H). ^{13}C NMR (125 MHz, DMSO) δ 162.3, 158.7, 153.5, 143.5, 132.7, 129.7, 129.1, 128.8, 128.5, 127.3, 126.7, 126.5, 123.1, 119.9, 119.2, 111.4, 50.6.

***N*-((2-hydroxynaphthalen-1-yl)(phenyl)methyl)benzamide (4i)**[40]

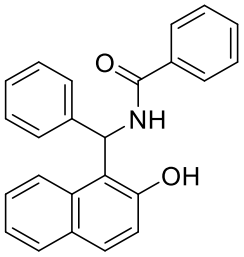

^{1}H NMR (500 MHz, DMSO-d_6) δ 10.34 (s, 1H), 9.03 (d, *J* = 8.5 Hz, 1H), 8.14 – 8.04 (m, 1H), 7.87 (d, *J* = 7.5 Hz, 2H), 7.84 (d, *J* = 8.0 Hz, 1H), 7.80 (d, *J* = 9.0 Hz, 1H), 7.55 (t, *J* = 7.5 Hz, 1H), 7.48 (t, *J* = 7.5 Hz, 3H), 7.33 – 7.24

(m, 7H), 7.20 (d, *J* = 7.0 Hz, 1H). ^{13}C NMR (125 MHz, DMSO-d_6) δ 165.7, 153.2, 142.0, 134.3, 132.3, 131.4, 129.5, 129.4, 128.6, 128.5, 128.4, 128.2, 127.1, 126.8, 126.5, 126.4, 122.7, 118.7, 118.3, 49.2.

_N_-((2-hydroxynaphthalen-1-yl)(_p_-tolyl)methyl)benzamide (4j)[40]

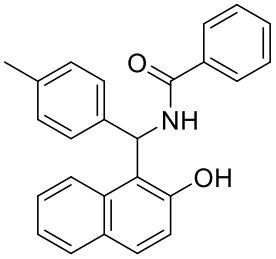

^{1}H NMR (500 MHz, DMSO-d_6) δ 10.33 (s, 1H), 9.01 (d, *J* = 8.5 Hz, 1H), 8.08 (d, *J* = 8.5 Hz, 1H), 7.86 (d, *J* = 7.5 Hz, 2H), 7.83 (d, *J* = 8.5 Hz, 1H), 7.79 (d, *J* = 9.0 Hz, 1H), 7.54 (t, *J* = 7.5 Hz, 1H), 7.49 (d, *J* = 7.5 Hz, 2H), 7.45 (d, *J* = 8.0 Hz, 1H), 7.33 – 7.28 (m, 2H), 7.25 (d, *J* = 9.0 Hz, 1H), 7.18 (d, *J* = 8.0 Hz, 2H), 7.08 (d, *J* = 8.0 Hz, 2H), 2.23 (s, 3H). ^{13}C NMR (125 MHz, DMSO-d_6) δ 165.7, 153.1, 139.0, 135.6, 134.4, 132.3, 131.4, 129.3, 128.8, 128.6, 128.5, 128.4, 127.1, 126.7, 126.4, 122.7, 118.7, 118.5, 49.1, 20.6.

_N_-((2-hydroxynaphthalen-1-yl)(4-methoxyphenyl)methyl)benzamide (4k)[41]

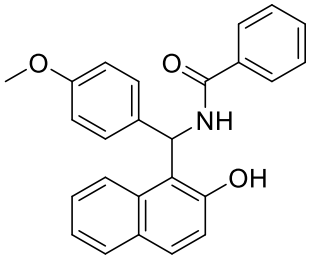

^{1}H NMR (500 MHz, DMSO-d_6) δ 10.33 (s, 1H), 9.02 (d, *J* = 8.5 Hz, 1H), 8.07 (d, *J* = 9.0 Hz, 1H), 7.88 – 7.81 (m, 3H), 7.79 (d, *J* = 9.0 Hz, 1H), 7.55 (t, *J* = 7.5 Hz, 1H), 7.49 (d, *J* = 8.0 Hz, 2H), 7.45 (d, *J* = 8.5 Hz, 1H), 7.31 (t, *J* = 7.5 Hz, 1H), 7.24 (d, *J* = 9.0 Hz, 2H), 7.20 (d, *J* = 8.5 Hz, 2H), 6.84 (d, *J* = 9.0 Hz, 2H), 3.68 (s, 3H). ^{13}C NMR (125 MHz, DMSO-d_6) δ 165.4, 158.0, 153.1, 134.4, 133.9, 132.2, 131.4, 129.2, 128.6, 128.5, 128.4, 127.7, 127.1, 126.7, 122.7, 118.7, 118.4, 113.6, 55.0, 48.1.

_N_-((4-fluorophenyl)(2-hydroxynaphthalen-1-yl)methyl)benzamide (4l)[29]

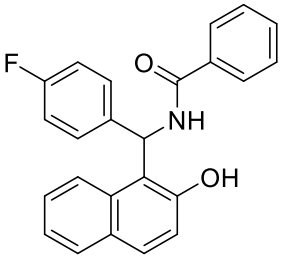

^{1}H NMR (500 MHz, DMSO-d_6) δ 10.39 (s, 1H), 9.05 (d, *J* = 8.5 Hz, 1H), 8.09 (d, *J* = 8.5 Hz, 1H), 7.88 (d, *J* = 7.0 Hz, 2H), 7.84 (d, *J* = 8.0 Hz, 1H), 7.81 (d, *J* = 9.0 Hz, 1H), 7.54 (t, *J* = 7.0 Hz, 1H), 7.48 (t, *J* = 7.5 Hz, 3H), 7.34 – 7.30 (m, 4H), 7.27 (d, *J* = 8.5 Hz, 1H), 7.11 (t, *J* = 8.5 Hz, 2H). ^{13}C NMR (125 MHz, DMSO-d_6) δ 165.8, 160.1 (d, *J* = 240.8 Hz), 153.2, 138.1 (d, *J* = 3.1 Hz), 134.3, 132.2, 131.5, 129.5, 128.7, 128.5, 128.4 (d, *J* = 8.3 Hz), 127.2, 126.9, 122.7, 118.7, 118.1, 114.9 (d, *J* = 21,0 Hz), 48.8.

Acknowledgements

This research was funded by University of Science, VNU-HCM, under grant number T2023-114.

Supplementary Material

Copies of ^{1}H NMR and ^{13}C NMR spectra of the synthesized compounds are available in the supplementary material file associated with this paper.

References

1. M. A. Bodaghifard, M. Hamidinasab and N. Ahadi, *Curr. Org. Chem.*, 2018, **22**, 234. https://doi.org/10.2174/1385272821666170705144854
2. H.-J. Xu, X. Wan, Y. Geng and X.-L. Xu, *Curr. Org. Chem.*, 2013, **17**, 1034.https://doi.org/10.2174/1385272811317100006
3. M. Fallah-Mehrjardi, *Mini-rev. Org. Chem.*, 2017, **14**, 122.https://doi.org/10.2174/1570193X14666170206144158
4. X. Zhang, X. He, S. Zhao and Reviews, *Green Chem. Lett. Rev.*, 2021, **14**, 85.https://doi.org/10.1080/17518253.2020.1862312
5. J. Ju, Y. Chen, Z. Liu, C. Huang, Y. Li, D. Kong, W. Shen and S. Tang, *Chin. Chem. Lett.*, 2023, **34**, 107820.https://doi.org/10.1016/j.cclet.2022.10782
6. A. Domling, W. Wang and K. Wang, *Chem. Rev.*, 2012, **112**, 3083.https://doi.org/10.1021/cr100233r
7. B. H. Rotstein, S. Zaretsky, V. Rai and A. K. Yudin, *Chem. Rev.*, 2014, **114**, 8323.https://doi.org/10.1021/cr400615v
8. S. Zandieh, N. Nami and Z. Hossaini, *Iran J. Chem. Chem. Eng.* , 2019, **38**, 27.https://doi.org/10.30492/ijcce.2019.31988
9. E. Ezzatzadeh and Z. Hossaini, *Nat. Prod. Res.*, 2020, **34**, 923.https://doi.org/10.1080/14786419.2018.1542389
10. N. Azizi and M. Edrisi, *Res. Chem. Intermed.*, 2017, **43**, 379.https://doi.org/10.1007/s11164-016-2628-2
11. A. Olyaei and M. Sadeghpour, *RSC Adv.*, 2019, **9**, 18467.https://doi.org/10.1039/C9RA02813G
12. A. Zare, *Org. Prep. Proced. Int.*, 2012, **44**, 82.https://doi.org/10.1080/00304948.2012.643199
13. C. Cardellicchio, M. A. M. Capozzi and F. Naso, *Tetrahedron: Asymmetry*, 2010, **21**, 507.https://doi.org/10.1016/j.tetasy.2010.03.020
14. G. S. Amitha and S. Vasudevan, *Polyhedron*, 2020, **190**, 114773. https://doi.org/10.1016/j.poly.2020.114773
15. M. A. Zolfigol, S. Baghery, A. R. Moosavi-Zare and S. M. Vahdat, *RSC Adv.*, 2015, **5**, 32933.https://doi.org/10.1039/C5RA03241E
16. H. Moghanian, A. Mobinikhaledi, A. G. Blackman and E. Sarough-Farahani, *RSC Adv.*, 2014, **4**, 28176.https://doi.org/10.1039/C4RA03676J
17. G. S. Amitha, V. K. Rajan, B. Amritha, K. Muraleedharan and S. Vasudevan, *J. Photochem. Photobiol. A*, 2019, **382**, 111904.https://doi.org/10.1016/j.jphotochem.2019.111904
18. H. R. Shaterian, H. Yarahmadi and M. Ghashang, *Tetrahedron*, 2008, **64**, 1263.https://doi.org/10.1016/j.tet.2007.11.070

19. M. Ghandi, A. Olyaei and S. Raoufmoghaddam, *Synthetic Communications*, 2008, **38**, 4125-4138.10.1080/00397910802279860
20. M. Nasr-Esfahani, M. Montazerozohori and M. Taei, *C. R. Chim.*, 2016, **19**, 986.https://doi.org/10.1016/j.crci.2016.02.003
21. T. Akbarpour, A. Khazaei, J. Yousefi Seyf and N. Sarmasti, *Appl. Organomet. Chem.*, 2021, **35**, e6361.https://doi.org/10.1002/aoc.6361
22. J. Rakhtshah and F. Yaghoobi, *Dalton Trans.*, 2019, **48**, 16268.https://doi.org/10.1039/C9DT03604K
23. A. Deepam and J. Viswanadhan, *Orient. J. Chem.*, 2017, **33**, 1354.https://doi.org/10.13005/ojc/330336
24. J. Safari and Z. Zarnegar, *J. Mol. Catal. A Chem.* , 2013, **379**, 269.https://doi.org/10.1016/j.molcata.2013.08.028
25. M. Hajjami, F. Ghorbani and F. Bakhti, *Appl. Catal.*, 2014, **470**, 303.https://doi.org/10.1016/j.apcata.2013.11.002
26. A. R. Hajipour, Y. Ghayeb, N. Sheikhan and A. E. Ruoho, *Tetrahedron Lett.*, 2009, **50**, 5649.https://doi.org/10.1016/j.tetlet.2009.07.116
27. A. Zali and A. Shokrolahi, *Chin. Chem. Lett.*, 2012, **23**, 269.https://doi.org/10.1016/j.cclet.2011.12.002
28. M. Forouzani and H. Ghasemnejad-Bosra, *Arab. J. Chem*, 2016, **9**, S752.https://doi.org/10.1016/j.arabjc.2011.08.002
29. K. S. Niralwad, B. B. Shingate and M. S. Shingare, *Chin. Chem. Lett.*, 2011, **22**, 551.https://doi.org/10.1016/j.cclet.2010.11.018
30. S. M. Patil, R. Tandon, N. Tandon, I. Singh, A. Bedre and V. Gade, *RSC Advances*, 2023, **13**, 17051-17061.10.1039/D3RA01522J
31. M. Mokhtary and M. Torabi, *Journal of Saudi Chemical Society*, 2017, **21**, S299-S304.https://doi.org/10.1016/j.jscs.2014.03.009
32. J. Rakhtshah, B. Shaabani, S. Salehzadeh and N. Hosseinpour Moghadam, *Bioorganic Chemistry*, 2019, **85**, 420-430.https://doi.org/10.1016/j.bioorg.2019.01.022
33. H. R. Shaterian, K. Azizi and N. Fahimi, *Arab. J. Chem.*, 2017, **10**, S42.https://doi.org/10.1016/j.arabjc.2012.07.006
34. K. Hemalatha, G. Madhumitha, A. Kajbafvala, N. Anupama, R. Sompalle and S. Mohana Roopan, *J. Nanomater.*, 2013, **2013**, 341015.https://doi.org/10.1155/2013/341015
35. H. Bae, T. Ahmad, I. Rhee, Y. Chang, S.-U. Jin and S. Hong, *Nanoscale Res. Lett.*, 2012, **7**, 44.https://doi.org/10.1186/1556-276X-7-44
36. M. S. Reza, S. Afroze, M. S. A. Bakar, R. Saidur, N. Aslfattahi, J. Taweekun and A. K. Azad, *Biochar*, 2020, **2**, 239.https://doi.org/10.1007/s42773-020-00048-0
37. Y. Wei, B. Han, X. Hu, Y. Lin, X. Wang and X. Deng, *Procedia Eng.*, 2012, **27**, 632.https://doi.org/10.1016/j.proeng.2011.12.498
38. Y. Jiang, S. Gao, Z. Li, X. Jia and Y. Chen, *Mater. Sci. Eng. B*, 2011, **176**, 1021.https://doi.org/10.1016/j.mseb.2011.05.023
39. J. Rakhtshah, H. Ghaderi, F. Yaghoobi, S. Baghery and B. Shaabani, *Mater. Chem. Phys.*, 2020, **239**, 121985.https://doi.org/10.1016/j.matchemphys.2019.121985
40. N. R. Rode, A. A. Tantray, A. V. Shelar, R. H. Patil and S. S. Terdale, *Res. Chem. Intermed.*, 2022, **48**, 2391.https://doi.org/10.1007/s11164-022-04723-8
41. M. Wang, Y. Liang, T. Zhang and J. Gao, *Chin. J. Chem.*, 2011, **29**, 1656.https://doi.org/10.1002/cjoc.201180296